Quantum Dot Assembly Driven by Electrochemically Generated Metal-ion Crosslinkers

Chathuranga C. Hewa-Rahinduwage, [a] Karunamuni L. Silva, [a] Stephanie L. Brock,*[a] Long Luo*[a]

[a] Department of Chemistry, Wayne State University, Detroit, MI 48220, U. S. A.

ABSTRACT: Control of nanoparticle assembly is a critical enabler for fabricating nanostructures capable of complex, system-level functionality. Here, we report a facile electrochemical method for assembling quantum dots (QDs) into mesoporous gels directly onto an electrode surface using localized, in situ generated metal ion crosslinkers (Ni^{2+}, Co^{2+}, Ag^+, or Zn^{2+}) within a colloidal solution of metal chalcogenide nanoparticles capped with ligands featuring pendant carboxylate groups. A mechanistic study reveals a critical stoichiometry of 0.5 metal ions: 1 QD in solution is required to trigger metal ion-mediated electrogelation (ME-gelation), representing a much lower concentration of metal ions than is needed for initiating crosslinking throughout an entire volume of solution (>26 metal ions: 1 QD in solution). The application of the ME gelation approach for the fabrication of QD-based electronic devices is demonstrated by electrochemical patterning of QD gels onto a printed circuit board chip.

INTRODUCTION

In the past two decades, advances in nanoparticle synthetic methods have dramatically expanded the library of nanoparticles, and consequently, exquisitely tailored physicochemical properties available for exploitation.[1-3] Despite our ability to generate individual nanoscale blocks with various compositional, structural, morphological, and surface properties, our ability to combine these components into multiscale architectures capable of system-level functionality is in its infancy.[4-7] Colloidal gel formation via sol-gel methods represents a versatile strategy for achieving nanoparticle assembly into 3-D interconnected networks across a range of length scales, from nanometer to meter, while retaining the intrinsic properties of the initial nanoscale building blocks.[8] The highly porous, 3-D connected gel network maximizes contact with the environment, making nanoparticle gels well-suited for sensing and catalysis applications.[9-15] Moreover, sol-gel methods are also amenable to thin film deposition and patterning.[16-17]

While traditionally applied to oxides, sol-gel methods have been developed for the assembly of metal chalcogenide nanoparticles, enabling the formation of quantum dot (QD) colloidal gels that retain the intrinsic size-dependent optoelectronic properties of the components.[18-24] The original (standard) approach to gelation of metal chalcogenide QDs involves chemical oxidation of thiolate-capped QDs (irreversible ligand removal) followed by oxidative assembly due to the formation of inter-particle dichalcogenide bonds.[19] This approach is amenable to thin-film deposition, patterning via ink-jet printing and can also be performed using electrochemical oxidation.[20, 25-26] However, the dichalcogenide linkages are not stable in a reducing environment, limiting conditions under which they can be deployed. An alternate approach to QD gelation that circumvents redox instability is to use coordinate bonds between Lewis acid metal cationic linkers and Lewis base functionalities pendant on surface capping ligands. This approach has been previously established for nanoparticle gelation, with flexibility enabled by the ability to tune the chain length of the pendant ligand, the pendant coordination site and geometry (carboxylate, imidazolate, etc.), and the identity of the metal ion.[21-24] However, metal-ion mediated assembly to form gels and aerogels is typically a batch process involving the introduction of metal ions to a colloidal sol, forming macroscale objects with dimensions and shapes defined by the mold. Such methods do not enable the introduction of fine detail to the QD gel form. To address this challenge, we demonstrate herein the electrochemically-driven formation of metal-ion crosslinked QD gel structures *on demand* by localized delivery of the metal ion from the electrode surface.

RESULTS AND DISCUSSION

To achieve metal ion-mediated electrogelation (ME-gelation) in lieu of oxidative electrogelation (OE-gelation), we need a metal with a relatively low oxidation potential to enable the delivery of ions under conditions that will not directly oxidize the QDs. Ni was chosen for proof of principle because its oxidation potential (-0.25 V vs. SHE) is significantly more negative than the potential for OE gelation (1.5 V vs. SHE).[20] During ME-gelation, a positive potential is applied at a Ni electrode to release Ni^{2+} ions into the colloidal sol of QDs capped with thiolate ligands, such as thioglycolate (TGA), to produce QD ME-gels via metal ion-carboxylate coordination (**Figure 1a**).
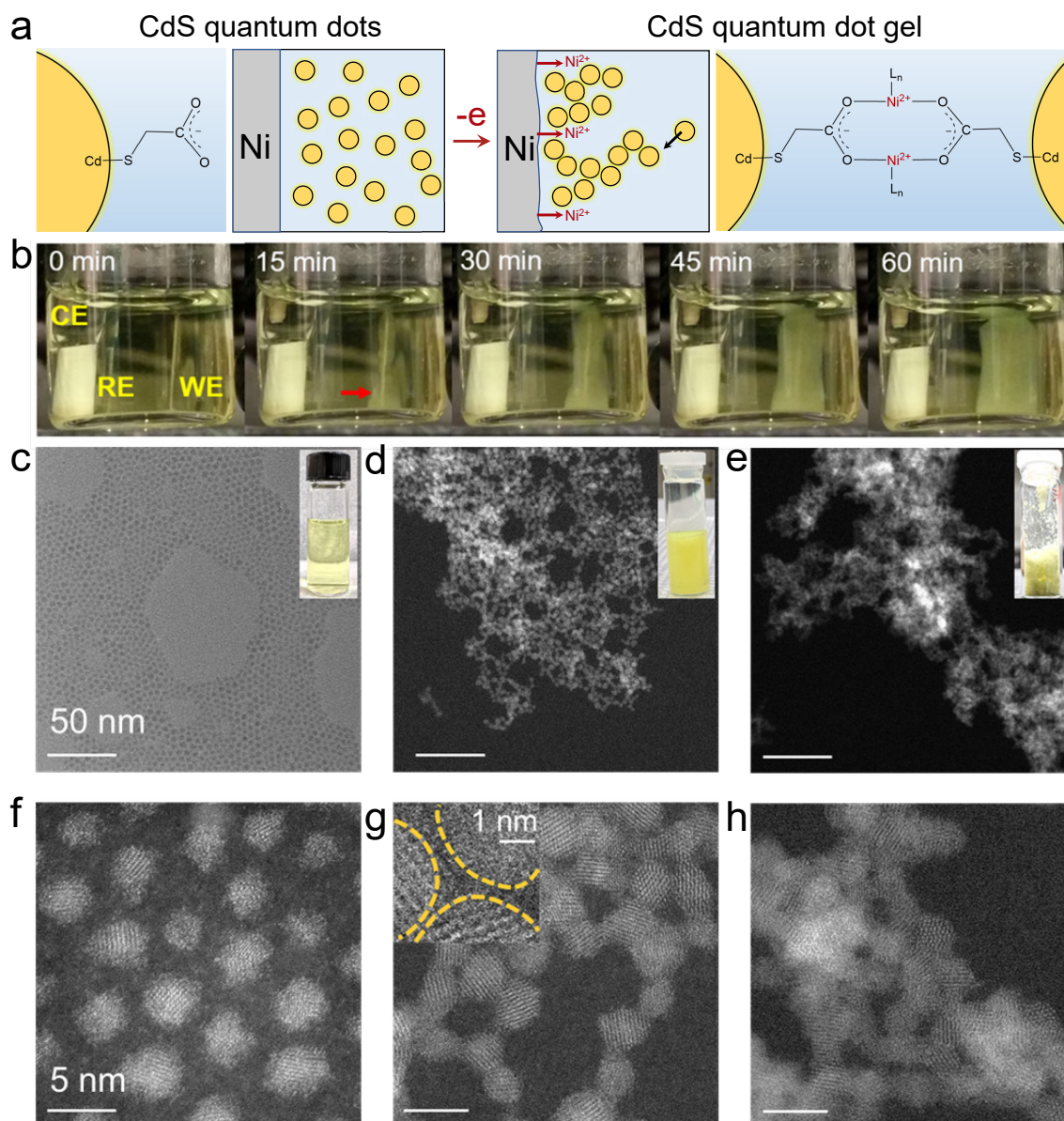
Figure 1. Metal ion-mediated electrogelation (ME-gelation) of QDs. a, Schematic of ME-gelation. Electrooxidation of a Ni electrode generates Ni ions. The released Ni ions crosslink QDs capped with thiolate ligands such as thioglycolate (TGA) into a QD gel network by coordinating the carboxylate groups with Ni ions in a bridging bidentate geometry. b, CdS QD gel formation on a Ni anode with time at a potential of 0.5 V vs Ag/AgCl/sat. KCl reference electrode. c-e, Low-resolution TEM and STEM images of CdS QDs, wet gel and aerogel, respectively. Insets show the photographs of each material. f-h, High-magnification STEM images of CdS QDs, wet gel and aerogel, respectively. The inset in g shows the gap between QDs in the gel network.

We first synthesized nearly monodisperse sols of TGA-capped CdS QDs with an average diameter of 3.4 ± 0.7 nm (**Figure 1c, f** and **Figure S1**) using a modified hot injection method.[27] ME-gelation of CdS QDs was initiated by applying a potential of 0.5 V vs. Ag/AgCl/sat. KCl at a Ni wire electrode immersed in the CdS QD solution. A thin layer of CdS QD gel was first observed on the Ni anode surface after ~15 mins, and the gel growth continued for one hour (**Figure 1b**). The electrode potential of 0.5 V is insufficient to drive direct oxidative gelation of TGA-capped CdS QDs (**Figure S2**).[20] ME-gelation of CdS QDs capped with long-chain thiolates such as 11-mercaptoundecanoate (MUA) was also observed at ~0.5 V (**Figure S3**), indicating ME-gelation is solely controlled by the oxidation of Ni to Ni^{2+} ions and

independent of the QD ligand chain length. The inductively coupled plasma mass spectrometry analysis of the CdS ME-gels prepared from TGA- and MUA-capped CdS QDs also shows similar Ni^{2+}/QD ratios of 153 and 150, respectively (see **Experimental Section**).

We investigated the structure and connectivity of the QDs in the ME-gel using transmission electron microscopy (TEM). **Figure 1c-e** shows the low-magnification TEM and STEM micrographs of CdS QDs, wet gel, and aerogel, respectively. Both the wet gel and aerogel show a three-dimensional mesoporous network with pore sizes between 2 to 50 nm. Individual CdS QD building blocks were discernible in the high-magnification STEM micrographs of
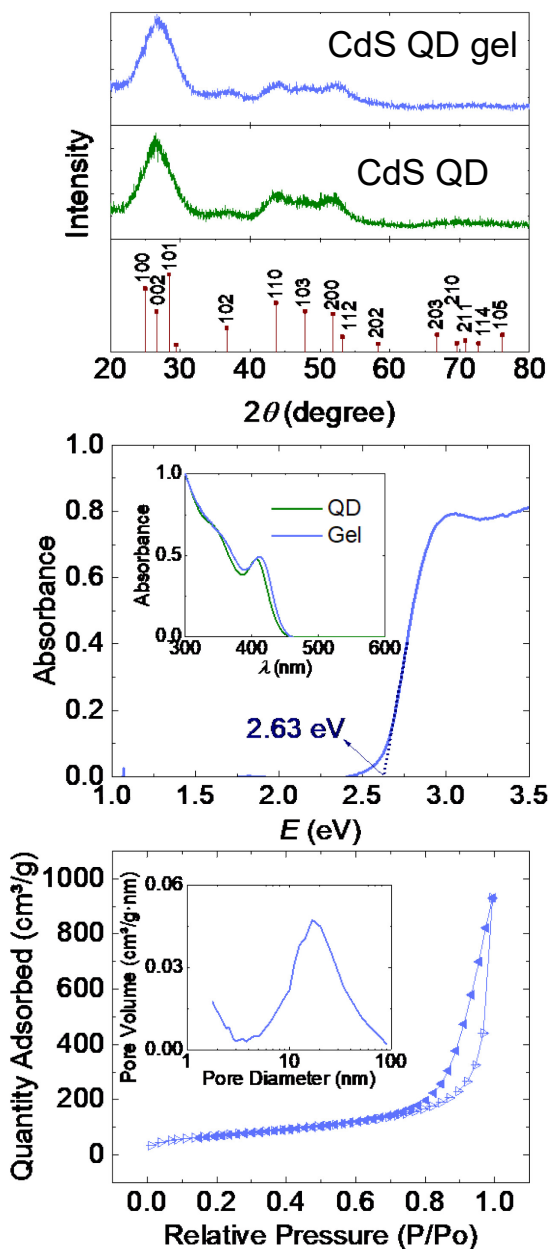
Figure 2. a, Powder X-ray diffraction (PXRD) patterns of CdS QD ME-aerogel and CdS QDs; the hexagonal CdS (wurtzite) PXRD pattern is shown as a reference (stick diagram; PDF 00-001-0780). b, Diffuse reflectance spectrum of a CdS QD ME-aerogel; the UV/Vis spectra of the CdS QDs and CdS QD ME-aerogel is shown in the inset. c, N_2 adsorption−desorption isotherms and BJH pore size distribution plot (inset) for the CdS QD ME-aerogel.

CdS QD gels, which kept the same size of ∼3 nm as the QD precursors (**Figure 1f-h** and **Figure S1**). Notably, CdS QDs in the gel are sometimes separated by ∼0.5 nm (**Figure 1g inset**), which was not observed in CdS QD gels prepared by OE-gelation (**Figure S4**). The separation between QDs becomes more pronounced for CdS QD ME-gels prepared from MUA-capped CdS QDs (∼1-1.5 nm) since MUA has a longer carbon chain than TGA (C11 vs. C2; **Figure S5**), confirming the proposed connection between QDs via a ligand-Ni^{2+}-ligand linkage. The Ni^{2+}-carboxylate coordination was further confirmed by the dispersion of ME-gels in the presence of ethylenediamine-tetraacetic acid (EDTA), which competes

with carboxylate-terminated thiolate ligands for binding with Ni^{2+}, disrupting the Ni^{2+}-carboxylate coordination (**Figure S6**). The infrared spectrum of the ME-gel in **Figure S7** shows a wavenumber difference of 173 cm^{-1} between the asymmetric and symmetric stretching vibrations of the carboxylate group, suggesting a bridging bidentate coordination between Ni^{2+} and carboxylates (**Figure 1a**).[28]

The crystallinity of the CdS QD ME-aerogel was characterized using powder X-ray diffraction (PXRD). The PXRD peak locations and peak breadths for the gel match the CdS QDs (**Figure 2a**), suggesting the QD structure and crystallite size is not affected by the ME-gelation process. This finding is consistent with the TEM results in **Figure 1f-h**.

We further measured the optical properties of the CdS QD ME-gels using UV-Vis and diffuse reflectance spectroscopy. The UV-Vis spectra of CdS QD and gel in **Figure 2b, inset** show the first excitonic peak only slightly red-shifted by 4 nm for the CdS QD gel relative to the QDs. The diffuse reflectance spectrum of the gel in **Figure 2b** shows a bandgap of 2.63 eV, significantly larger than the bandgap of bulk CdS (2.42 eV). Both results suggest the QD ME-gel remains quantum-confined even though they are linked together via the Ni^{2+} crosslinker in a 3-D network.

The surface area of CdS QD ME-aerogel was measured by nitrogen adsorption-desorption isotherms using the Brunauer–Emmett–Teller (BET) model.[29] A type-IV isotherm, characteristic of a mesoporous network, was observed (**Figure 2c**). The BET surface area was measured to be 258 m^2/g. The Barrett–Joyner–Halenda (BJH) model was used to obtain the average pore size distribution (**Figure 2c, inset**).[30] The average BJH pore diameter and the cumulative pore volume are 21 nm and 1.4 cm^3/g, respectively. Both the BET surface area and BJH cumulative pore volume are slightly larger (∼20%) than those of typical OE-gels prepared from similarly-sized CdS QDs (**Table S1**).[20]

For comparison, gelation was also performed by direct introduction of Ni^{2+} ions to a sol of MUA-capped CdS to produce an MC-gel (**Figure S8**). Intriguingly, while the MC-gel is very similar to the ME-gel when comparing electron microscopy, powder diffraction, and optical spectroscopic data, the MC-gel has a dramatically lower surface area (65 m^2/g, **Figure S8** and **Table S1**). We noted that the Ni^{2+}/QD ratio determined by ICP-MS in the MC-aerogel was much higher than that for the ME-aerogel (315 vs.150) and hypothesized that the number of crosslinkers might impact the gel structure. We were able to produce dramatically lower ratios (Ni^{2+}/QD = 26) by decreasing the Ni^{2+}/QD ratio in the synthesis (83 vs. 2611), demonstrating that a significant range of composition can be achieved in the system. However, the surface area was not improved (70 m^2/g), suggesting the kinetic process of assembly is quite different for the ME- and MC-gels.

To further understand the ME-gelation process, we carried out a potential-dependent study. An electrode potential of 0.3, 0.4, 0.5, or 0.6 V was applied at the Ni electrode to initiate ME-gelation. All these potentials are sufficient to oxidize Ni to Ni^{2+}, but we did not observe ME-gel formation at 0.3 V even after 1 h (**Figure 3a**). More interestingly,
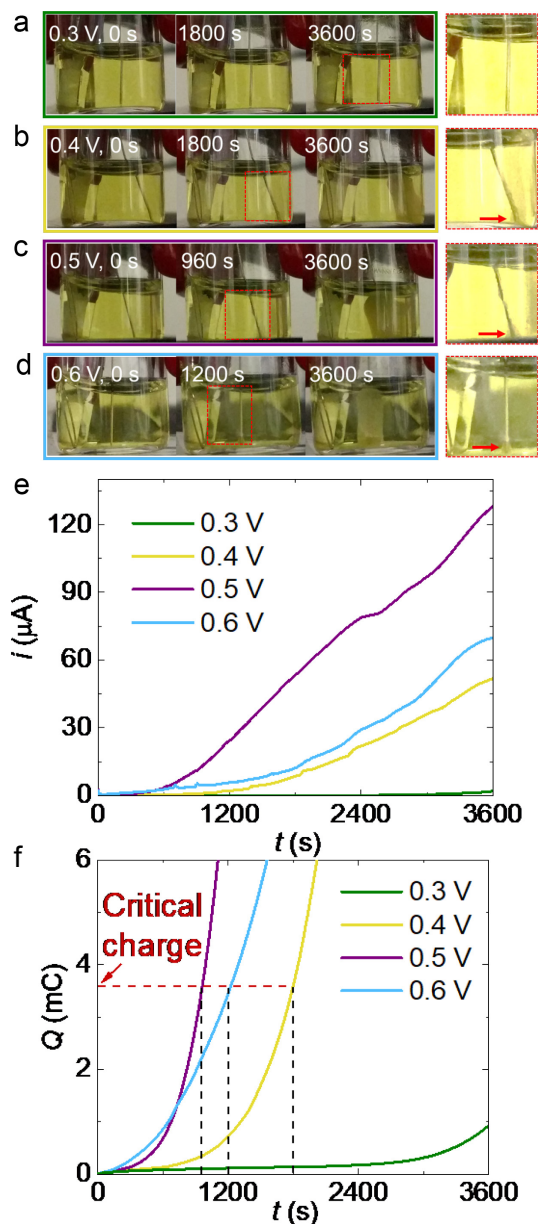
Figure 3. a-d, Photographs of CdS QD ME-gelation as a function of time at different applied electrode potentials from 0.3 V to 0.6 V vs Ag/AgCl/sat. KCl electrode. An expanded view of the working electrode at each gelation starting point is shown in the red-dashed box on the right. e and f, Current-time and charge-time traces for the corresponding ME-gelation potentials in a-d. Black dotted lines connect the observed gelation induction times to the charge-time traces.

there was a certain induction time required for the gel to appear on the electrode at potentials higher than 0.3 V, and the induction time is not positively correlated with the applied potential. For example, the gel was visible to the naked eye at 960 s at 0.5 V but did not appear until 1200 s at 0.6 V (**Figure 3c** and **d**). Such growth behavior of ME-gels is distinguishable from that of OE-gels, where gel growth is seen immediately upon the application of a sufficient electrode potential, and the OE-gel growth rate increases with the applied potential. A closer look at the current-time traces at

various potentials in **Figure 3e** shows the current continuously increased with time during the ME-gelation. The increasing current results from the increase of electrode surface roughness during the anodic dissolution of the Ni electrode (**Figure S9**). Because anodic dissolution of transition metals such as Ni is well-known to be nonlinear and sometimes chaotic due to a complex interplay of the underlying passivation (oxide formation) and activation (oxide dissolution) surface processes,[31-34] the faradaic current and electrode potential did not show a reproducible positive correlation. However, we discovered a constant critical charge of 3.6 mC for ME-gelation after analyzing the total charge at each induction time when the gels started appearing on the Ni electrode (**Figure 3f**). Because Ni electrodissolution is the only anodic reaction at the electrode potential of ≤ 0.6 V (**Figure S10**), this critical charge value means a certain level of Ni^{2+} in the solution is required to trigger the ME-gelation. We estimated the total number of Ni^{2+} ions released during the induction time using Faraday's laws and divided the obtained value by the total number of QDs in the solution, giving an overall stoichiometry of 0.5 Ni^{2+}: 1 QD in solution for triggering ME-gelation. However, because the ions are generated and consumed in close proximity to the electrode, the localized concentration of Ni2+ relative to CdS QD is expected to be much greater.
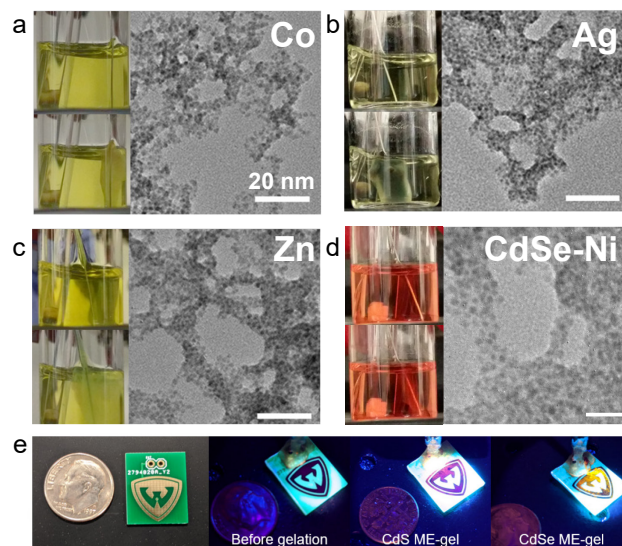

Figure 4. ME-gelation of MUA-capped CdS QDs using different metal anodes a-c, Co, Ag, and Zn, respectively, at 1.2 V and d, MUA-capped CdSe QDs using a Ni electrode. To the left of the TEM images are the corresponding photographs taken at 0 minutes (top) and 15 minutes (bottom) after the potential application. e, Photographs, from left to right: imaging under ambient light, a printed circuit board (PCB) chip patterned with an Au-coated electrode; imaging under ultraviolet light, the PCB chip after electrodeposition of Ni onto the electrode (before gelation), and after ME gelation of CdS, and CdSe QDs. A U.S. 10 cent coin (18 mm diameter) is included for scale.

To better understand the localized metal ion-mediated electrogelation process relative to bulk-phase gelation achieved by adding metal salts to initiate crosslinking, we added aliquots of Ni^{2+} into a TGA-capped CdS QD sol and monitored the process by dynamic light scattering (**Figure S11a**). Rapid growth occurs at a Ni^{2+}:QD ratio greater than

26, but no more than 33. Visual inspection of the cuvette after the reaction showed gel fragments throughout the volume, consistent with the initiation of gelation (**Figure S11b**). These data suggest that the relative concentration of Ni^{2+}:QD must be much larger to initiate gelation (at least 50 x larger) at the electrode surface than that indicated by the critical charge.

The ME-gelation method is amenable to the use of other metals with low oxidation potentials such as Co, Ag, and Zn; and other nanoparticles such as CdSe QDs, as shown in **Figure 4a-d.** Moreover, the method can be used to pattern QD gels directly onto a printed circuit board (PCB) chip (**Figure 4e** and **Figure S12**). QD patterning on PCBs is an essential step in fabricating QD-based electronic devices such as light-emitting diode displays.[35-37] As shown in **Figure 4e**, the ME-gels uniformly covered the patterned electrode and, most importantly, remained highly emissive under ultraviolet light.

In conclusion, we have demonstrated a new QD gelation method by electrochemically generating metal ions to crosslink QDs capped with ligands that have pendant carboxylate functionalities. The versatility of the electrochemical assembly method in terms of nanoparticle and crosslinker identity, combined with the ability to directly write these structures onto patterned electrodes, suggests this approach may be amenable to rapid production of more complex, functional architectures, such as multiplexed sensors.

EXPERIMENTAL SECTION.

Chemicals and Materials. Tetrabutylammonium hexafluorophosphate [TBAPF$_6$, 98%], was purchased from Sigma-Aldrich; OmniTrace nitric acid [HNO$_3$, 67-71%] was purchased from Millipore Sigma; nickel sulfate 6-hydrate [NiSO$_4$·6H$_2$O, 99.7%] powder was purchased from Mallinckrodt chemicals; Ni(II) chloride hexahydrate [NiCl$_2$·6H$_2$O, 99%] was purchased from Avantor chemicals; ethylenediamine tetra-acetic acid, disodium salt dihydrate [Na$_2$EDTA, >99%] was purchased from Fisher Scientific chemicals; Ni wire [0.25 mm diameter, 99.98%], Co wire [0.25 mm diameter, 99.995%], and Pt wire [0.25 mm diameter, 99.99%] were purchased from Alfa-Aesar; Ag wire [0.010" diameter, 99.99%] was purchased from A-M Systems; deionized water [DI, PURELAB, 18.2 MΩ· cm, TOC < 3 ppb] was used to clean the electrodes and prepare aqueous solutions.

Synthesis of CdS and CdSe QDs. CdS and CdSe QDs were synthesized by following modified hot injection methods, as described in the supporting information.[27, 38 39]

QD ligand exchange with thioglycolic acid (TGA) and mercaptoundecanoic acid (MUA). Ligand exchange was achieved by following standard prototocls (see Supporting Information). TGA- and MUA-capped QDs were finally dispersed in methanol, and concentrations were adjusted by serial dilution to 40 µM concentration of QDs based on comparison of UV-Vis spectra to published absorptivity data.[40]

Electrogelation of QDs. All the ME-gelation experiments were carried out inside a 3-electrode cell. The reference electrode was Ag/AgCl/sat. KCl and the counter electrode was a Pt wire (folded to increase the surface area over the working electrode wire). The QD dispersion (40 µM, 900 µL) was mixed with a TBA-PF$_6$ electrolyte solution (0.1 M, 100 µL) to get a QD concentration of 36 µM, just before the gelation. Both the reference electrode and the counter electrode were washed with DI water and methanol, dried with a paper wipe, and immersed in the QD solution for gelation.

ME-gelation. The working electrode for the ME-gelation was a Ni wire. The wire was scratch polished using 400-grit 3M sandpaper to expose a fresh layer of material. The wire was then washed with DI water and placed in a 15 mL centrifuge vial with DI water. The vial was sonicated for 1 minute and rewashed using plenty of DI water. Next, the wire was cleaned using methanol, dried, and immersed in the QD solution for gelation. The gelation setup was always maintained under low-light conditions, and a digital camera was used to capture the images every minute. The required potential was applied using a CHI 650E potentiostat. The *iR* drop was compensated manually after measuring the solution resistance using a potentiostat function. After the gelation, the Ni wire was removed carefully without damaging the gel monolith. The remaining QD dispersion was pipetted out, and 3 mL of acetone was added immediately to keep the gel wet. This acetone solution was exchanged with another 3 mL of acetone two more times. After the third acetone exchange, the gel was stored in the dark.

Co, Ag, and Zn wires were used to demonstrate the ME-gelation using different metals. MUA-capped CdS QDs were used for the study. MUA capped QDs required a higher potential of 1.6 V to start the OE-gelation. Therefore, 1.2 V was selected to demonstrate the ME-gelation for this set of experiments. The wires were cleaned following the same procedure used for Ni wire cleaning. Gelation was carried out in the same three-electrode setup described above for 15 minutes. CdSe QDs demonstrated lower stability at high potentials such as 1.2 V. Therefore, the ME-gelation of CdSe QDs was carried out using a Ni wire at 0.8 V for 30 minutes.

OE-gelation. The working electrode for the OE-gelation was a Pt wire. The wire was electropolished by running 50 cyclic voltammograms in 0.5 M H$_2$SO$_4$ at 0.1 V/s between 1.1 V and -0.23 V. The wire was first washed with plenty of water, next with methanol, and dried before immersed in the QD dispersion. The gelation setup was always maintained under low light conditions. The required potential was applied using a CHI 650E potentiostat after manually compensating the *iR* drop.

MC-gelation. For comparison to the ME-gelation method, the formation of a metal-ion crosslinked gel was performed by direct addition of Ni^{2+} ions (from $NiCl_2$) to a colloid of MUA-capped CdS (3.6 ± 0.4 nm diameter) to form a metal-induced chemical gel (MC-gel). The Ni^{2+} ion solution (0.05 M) was prepared by dissolving 0.30g of NiCl$_2$·6H$_2$O in 25.0 mL of absolute ethanol. 940 µL of freshly prepared 0.05 M Ni^{2+} ion solution was added to 3 mL of MUA-capped CdS QD solution (6 µM) dispersed in methanol, corresponding to a ratio of Ni^{2+}/ CdS QD = 2611. The mixture was shaken vigorously for 2 seconds, and gel formation occurred within 30 minutes. An MC gel was also produced from TGA-capped CdS QDs using a much lower Ni^{2+}/CdS QD ratio of 83. The wet gels were kept in the mother liquor in the dark in a desiccator for 24 h to prevent photooxidative gelation.

Aerogel preparation. Gels prepared for aerogel preparation were subjected to a prolonged solvent exchange with

acetone for five days (see Supporting Information). Super-critical drying was carried out using an SPI-DRY model CO_2 critical point dryer (CPD) connected to an ISOTEMP 10065 recirculating water bath. The 10 mL vial containing the wet gel was placed inside the drying chamber of the CPD and filled with acetone. The chamber was closed tightly, and liquid CO_2 was allowed to flow into the chamber by opening the valve on the top. After every 20 minutes, the liquid inside the chamber was replaced with a fresh portion of liquid CO_2. After 12 exchanges were completed (4 hours), the temperature of the water circulator was raised to 37 ^{0}C to reach the supercritical state. The chamber was kept at this condition for 1 hour, and the pressure was slowly released throughout ~ 30 minutes until it came to 1 atm.

Characterization of materials.

Electron microscope images (TEM and STEM) were taken using a JEOL 2010 and/or JEOL 3100R05 electron microscopes. Formvar/Carbon coated 200 mesh Cu grids (Ted Pella, USA) were used to prepare TEM samples. Particle sizes were analyzed using ImageJ 1.51j8 software.

Infrared Spectroscopy (IR) data were taken using a Bruker Tensor 27 FTIR spectrophotometer. The QD gels were prepared as KBr pellets before obtaining the data.

Powder X-ray diffraction (PXRD) data were collected on a Bruker D2 Phaser and the powder diffraction file (PDF) database of the International Center for Diffraction Data was used to identify the patterns.

Optical absorbance (UV/Vis) data were taken using a Shimadzu UV-1800 spectrometer. A quartz cuvette was used for the measurements. QDs (in methanol) and gels (in methanol/toluene mixtures) were sonicated for 30 minutes before the measurements to obtain a uniform dispersion.

Diffuse reflectance (DR) data were collected using a JASCO V-570 UV/VIS/NIR spectrometer. The aerogel sample was mixed with $BaSO_4$ before loading onto the solid sample holder. For the bandgap measurement, the Kubelka-Munk relationship was used to convert reflectance data to absorbance.

Nitrogen physisorption isotherms were collected on a Micrometrics ASAP 2020 analyzer at 77 K to determine the surface area and the pore size distribution of the aerogel. The aerogel samples were degassed for 14 hours at 150 ^{0}C. Brunauer–Emmett–Teller model and the Barrett-Joyner-Halenda model were used to calculate the surface area and the pore size distributions.

Inductively coupled plasma mass spectrometry (ICP-MS) was collected on an Agilent 7700x series instrument to determine Cd and Ni metal concentrations in ME and MC gel samples. Samples were digested in conc. nitric acid under sonication for 6 hours. The samples were then diluted using 2% nitric acid to obtain concentrations in the calibration range (0.5 ppb to 200 ppb).

Time-resolved dynamic light scattering (TR-DLS) measurements were performed on a Zetasizer Nano ZS instrument from Malvern Instruments. This contains a He–Ne laser beam at 633 nm and the detector positioned at 173°. The sample was suspended in methanol, and analysis was carried out at 25 ^{0}C. The Z-average hydrodynamic radius ($\bar{R}_h$) was determined using the Zetasizer software (6.2) provided by Malvern. $\bar{R}_h$ represents the size of a QD along with its surface-bound particles (surface ligands and solvent molecules around the particle). For the TR-DLS measurements, 2 mL of 1.52 μM TGA-CdS QD sol in methanol was pipetted into a disposable cuvette. After 120 seconds of equilibrium time, $\bar{R}_h$ data were acquired (corresponding to the native $\bar{R}_h$ of the QD sol). Then, the sequential addition of Ni^{2+} ions (4 aliquots, 5.0 μL of 5.0 mM Ni^{2+}) were carried out using a 20 μL pipette. After each addition, the sol was mixed using the pipette tip, and the lid of the instrument was quickly reclosed. Before each addition of Ni^{2+} ion, the $\bar{R}_h$ was monitored until a constant value was obtained.

EDTA dispersion study. 0.36 M EDTA solution was prepared by dissolving 0.263g of Na_2EDTA in 25.0 mL of ultrapure water, and the pH was adjusted to 8.5 using NaOH. 1 mL of EDTA solution was added to each vial containing OC, MC, or ME gels and mixed gently. As a control, H_2O was added to a separate set of vials containing the OC, MC, and ME gels.

Calculation of the Ni^{2+}/QD ratio in ME and MC gels. The Ni^{2+}/QD ratio in the MC- and ME-gel was estimated as follows. First, the QD diameter was determined using UV-Vis absorbance data.[40] Then, the mass of a single QD was calculated from the bulk CdS density (4.8 g/cm^3) and the QD diameter.[41] The number of Cd atoms per QD was calculated using the molecular mass of CdS and Avogadro's number. After obtaining the ratio of Ni and Cd in the gel samples using ICP-MS, we calculated the ratio of Ni^{2+}/QD in the gel by dividing it by the number of Cd atoms per QD.

Patterning of QDs on a PCB chip. The PCB chips patterned with a Wayne State University logo-shaped Au-coated electrode were purchased from the JLCPCB company (Shenzhen, China). Connector wires were attached to the circuit by soldering, and all the connections except the desired electrode surface were covered completely using a resistive epoxy resin. First, the PCB chip was cleaned with plenty of DI water and dried. A Ni^{2+} solution (0.5 M) was prepared by dissolving $NiSO_4 \cdot 6H_2O$ in water. The pH of the solution was adjusted to 3 using 1 M HCl. The PCB chip was immersed in this solution, and a Ni layer was electrodeposited onto the electrode at -1 V. After 15 minutes of deposition, the applied potential was discontinued, and the electrode surface was cleaned thoroughly using water and methanol. At this point, the gold surface turned grey due to the deposited Ni (Figure S12). After Ni deposition, the PCB chip was immersed in ~10 mL of ~36 μM QD dispersion. $TBAPF_6$ was added to get a final electrolyte concentration of ~10 mM. An Ag/AgCl/Sat. KCl reference electrode and a Pt foil counter electrode were used to carry out the QD patterning on the PCB chip. An electrode potential of 0.5 V was applied for a period of 30 minutes. Then, the PCB chip coated with the gel was removed from the solution. Unattached QDs were carefully washed away using methanol. The wet gel was allowed to dry into a xerogel in the lab ambient. The photoluminescence images of the PCB chip were collected in a dark room under UV light.

ASSOCIATED CONTENT

Supporting Information.

Details on the synthesis and ligand exchange of CdS and CdSe nanoparticles and solvent exchange of wet gels; size distributions of QDs before and after ME-gelation; photographs of TGA-capped CdS QD electrogelation at different electrode potentials using Ni and Pt wire electrodes; Photographs of ME-gelation of MUA-capped CdS QDs at 0.5 V vs Ag/AgCl/sat. KCl; STEM images of OE-gels prepared from TGA-capped CdS QDs; STEM image of ME-gels and OE-gels prepared from MUA-capped CdS QDs; EDTA dispersion study results; IR spectrum of CdS ME-gel; structural characterization results of MC-gels; SEM images of Ni wire before and after ME-gelation; Ni wire oxidation efficiency in methanol under different electrode potentials; time-resolved dynamic light scattering measurements of the MC-gelation process; photographs of QD patterning on a PCB chip; and comparison of surface area and pore size between CdS QD ME-aerogel, MC-aerogel, and the aerogel prepared by oxidative assembly methods. This material is available free of charge via the Internet at http://pubs.acs.org.

AUTHOR INFORMATION

Corresponding Author

*sbrock@chem.wayne.edu
*long.luo@wayne.edu

The authors declare no competing financial interest.

ACKNOWLEDGMENT

REFERENCES

1. Grzelczak, M.; Pérez-Juste, J.; Mulvaney, P.; Liz-Marzán, L. M., Shape control in gold nanoparticle synthesis. *Chem. Soc. Rev.* **2008,** *37* (9), 1783-1791.

2. Duan, H.; Wang, D.; Li, Y., Green chemistry for nanoparticle synthesis. *Chem. Soc. Rev.* **2015,** *44* (16), 5778-5792.

3. Mourdikoudis, S.; Liz-Marzán, L. M., Oleylamine in nanoparticle synthesis. *Chem. Mater.* **2013,** *25* (9), 1465-1476.

4. Zhong, Y.; Zhao, G.; Ma, F.; Wu, Y.; Hao, X., Utilizing photocorrosion-recrystallization to prepare a highly stable and efficient CdS/WS2 nanocomposite photocatalyst for hydrogen evolution. *Appl. Catal. B: Environ.* **2016,** *199*, 466-472.

5. Srivastava, S.; Santos, A.; Critchley, K.; Kim, K.-S.; Podsiadlo, P.; Sun, K.; Lee, J.; Xu, C.; Lilly, G. D.; Glotzer, S. C.; Kotov, N. A., Light-Controlled Self-Assembly of Semiconductor Nanoparticles into Twisted Ribbons. *Science* **2010,** *327* (5971), 1355-1359.

6. Velev, O. D.; Gupta, S., Materials Fabricated by Micro‐ and Nanoparticle Assembly – The Challenging Path from Science to Engineering. *Adv. Mater. (Weinheim, Ger.)* **2009,** *21* (19), 1897-1905.

7. Tan, W.; Li, Y.; Jiang, W.; Gao, C.; Zhuang, C., CdS Nanospheres Decorated with NiS Quantum Dots as Nobel-Metal-Free Photocatalysts for Efficient Hydrogen Evolution. *ACS Appl. Energy Mater.* **2020,** *3* (8), 8048-8054.

8. Matter, F.; Luna, A. L.; Niederberger, M., From colloidal dispersions to aerogels: How to master nanoparticle gelation. *Nano Today* **2020,** *30*, 100827.

9. Hüsing, N.; Schuber, U., Aerogels-Airy Materials: Chemistry, Structure and Properties. *Angew. Chem. Int. Ed.* **1998,** *37*, 22 – 45.

10. Rolison, D. R.; Long, J. W.; Lytle, J. C.; Fischer, A. E.; Rhodes, C. P.; McEvoy, T. M.; Bourga, M. E.; Lubersa, A. M., Multifunctional 3D Nanoarchitectures for Energy Storage and Conversion. *Chem. Soc. Rev.* **2009,** *38*, 226-252.

11. Huang, C.; Chen, X.; Xue, Z.; Wang, T., Effect of structure: A new insight into nanoparticle assemblies from inanimate to animate. *Sci. Adv.* **2020,** *6* (20), eaba1321.

12. C., B. N.; Anne‐Kristin, H.; Maria, V.; Marcus, R.; Paul, S.; Wilder, C. C.; Dirk, D.; Stefan, K.; Nikolai, G.; Alexander, E., Hydrogels and Aerogels from Noble Metal Nanoparticles. *Angew. Chem., Int. Ed.* **2009,** *48* (51), 9731-9734.

13. Liyanage, D. R.; Danforth, S. J.; Liu, Y.; Bussell, M. E.; Brock, S. L., Simultaneous Control of Composition, Size, and Morphology in Discrete Ni2–xCoxP Nanoparticles. *Chem. Mater.* **2015,** *27* (12), 4349-4357.

14. Huang, Z.-F.; Song, J.; Li, K.; Tahir, M.; Wang, Y.-T.; Pan, L.; Wang, L.; Zhang, X.; Zou, J.-J., Hollow Cobalt-Based Bimetallic Sulfide Polyhedra for Efficient All-pH-Value Electrochemical and Photocatalytic Hydrogen Evolution. *J. Am. Chem. Soc.* **2016,** *138* (4), 1359-1365.

15. Peng, W.; Li, Y.; Zhang, F.; Zhang, G.; Fan, X., Roles of Two-Dimensional Transition Metal Dichalcogenides as Cocatalysts in Photocatalytic Hydrogen Evolution and Environmental Remediation. *Ind. Eng. Chem. Res.* **2017,** *56* (16), 4611-4626.

16. Grosso, D.; Boissière, C.; Faustini, M., Thin Film Deposition Techniques. In *The Sol‐Gel Handbook*, 2015; pp 277-316.

17. Carretero-Genevrier, A.; Drisko, G. L.; Grosso, D.; Boissiere, C.; Sanchez, C., Mesoscopically structured nanocrystalline metal oxide thin films. *Nanoscale* **2014,** *6* (23), 14025-14043.

18. Rusch, P.; Zámbó, D.; Bigall, N. C., Control over Structure and Properties in Nanocrystal Aerogels at the Nano-, Micro-, and Macroscale. *Acc. Chem. Res.* **2020,** *53* (10), 2414-2424.

19. Arachchige, I. U.; Brock, S. L., Sol-gel methods for the assembly of quantum-dot monoliths. *Acc. Chem. Res* **2007,** *40*, 801-809.

20. Hewa-Rahinduwage, C. C.; Geng, X.; Silva, K. L.; Niu, X.; Zhang, L.; Brock, S. L.; Luo, L., Reversible Electrochemical Gelation of Metal Chalcogenide Quantum Dots. *J. Am. Chem. Soc.* **2020,** *142* (28), 12207-12215.

21. Lesnyak, V.; Voitekhovich, S. V.; Gaponik, P. N.; Gaponik, N.; Eychmüller, A., CdTe Nanocrystals Capped with a Tetrazolyl Analogue of Thioglycolic Acid: Aqueous Synthesis, Characterization, and Metal-Assisted Assembly. *ACS Nano* **2010,** *4*, 4090-4096.

22. Singh, A.; Lindquist, B. A.; Ong, G. K.; Jadrich, R. B.; Singh, A.; Ha, H.; Ellison, C. J.; Truskett, T. M.; Milliron, D. J., Linking Semiconductor Nanocrystals into Gel Networks through All-Inorganic Bridges. *Angew. Chem. Int. Ed. Engl.* **2015,** *54* (49), 14840-4.

23. Lesnyak, V.; Wolf, A.; Dubavik, A.; Borchardt, L.; Voitekhovich, S. V.; Gaponik, N.; Kaskel, S.; Eychmüller, A., 3D Assembly of Semiconductor and Metal Nanocrystals: Hybrid CdTe/Au Structures with Controlled Content. *J. Am. Chem. Soc.* **2011,** *133* (34), 13413-13420.

24. Hitihami-Mudiyanselage, A.; Senevirathne, K.; Brock, S. L., Bottom-Up Assembly of Ni2P Nanoparticles into Three-Dimensional Architectures: An Alternative Mechanism for Phosphide Gelation. *Chem. Mater.* **2014,** *26* (21), 6251-6256.

25. Korala, L.; Wang, Z.; Liu, Y.; Maldonado, S.; Brock, S. L., Uniform Thin Films of CdSe and CdSe(ZnS) Core(Shell) Quantum Dots by Sol–Gel Assembly: Enabling Photoelectrochemical Characterization and Electronic Applications. *ACS Nano* **2013,** *7* (2), 1215-1223.

26. Lübkemann, F.; Miethe, J. F.; Steinbach, F.; Rusch, P.; Schlosser, A.; Zámbó, D.; Heinemeyer, T.; Natke, D.; Zok, D.; Dorfs, D.; Bigall, N. C., Patterning of Nanoparticle-Based Aerogels and Xerogels by Inkjet Printing. *Small* **2019,** *15* (39), 1902186.

27. Davis, J. L.; Chalifoux, A. M.; Brock, S. L., Role of crystal structure and chalcogenide redox properties on the oxidative assembly of cadmium chalcogenide nanocrystals. *Langmuir* **2017,** *33* (37), 9434-9443.

28. Uddin, N.; Sirajuddin, M.; Uddin, N.; Tariq, M.; Ullah, H.; Ali, S.; Tirmizi, S. A.; Khan, A. R., Synthesis, spectroscopic characterization, biological screenings, DNA binding study and POM analyses of transition metal carboxylates. *Spectrochim. Acta A* **2015,** *140*, 563-574.

29. Gelb, L. D.; Gubbins, K., Characterization of porous glasses: Simulation models, adsorption isotherms, and the Brunauer–Emmett– Teller analysis method. *Langmuir* **1998,** *14* (8), 2097-2111.

30. Barrett, E. P.; Joyner, L. G.; Halenda, P. P., The determination of pore volume and area distributions in porous substances. I. Computations from nitrogen isotherms. *J. Am. Chem. Soc.* **1951,** *73* (1), 373-380.

31. dos Santos, C. G. P.; Machado, E. G.; Kiss, I. Z.; Nagao, R., Investigation of the Oscillatory Electrodissolution of the Nickel‐Iron Alloy. *J. Phys. Chem. C* **2019,** *123* (39), 24087-24094.

32. Gregori, J.; Garcia-Jareño, J. J.; Gimenez-Romero, D.; Vicente, F., Anodic Dissolution of Nickel Across Two Consecutive Electron Transfers: Calculation of the Ni(I) Intermediate Concentration by means EQCM. *ECS Trans.* **2019,** *2* (9), 83-97.

33. Cioffi, A. G.; Scott Martin, R.; Kiss, I. Z., Electrochemical oscillations of nickel electrodissolution in an epoxy-based microchip flow cell. *J. Electroanal. Chem.* **2011,** *659* (1), 92-100.

34. Wickramasinghe, M.; Kiss, I. Z., Effect of temperature on precision of chaotic oscillations in nickel electrodissolution. *Chaos* **2010,** *20* (2), 023125.

35. Yang, J.; Hahm, D.; Kim, K.; Rhee, S.; Lee, M.; Kim, S.; Chang, J. H.; Park, H. W.; Lim, J.; Lee, M.; Kim, H.; Bang, J.; Ahn, H.; Cho, J. H.; Kwak, J.; Kim, B.; Lee, C.; Bae, W. K.; Kang, M. S., High-resolution patterning of colloidal quantum dots via non-destructive, light-driven ligand crosslinking. *Nat. Commun.* **2020,** *11* (1), 2874.

36. Azzellino, G.; Freyria, F. S.; Nasilowski, M.; Bawendi, M. G.; Bulović, V., Micron‐Scale Patterning of High Quantum Yield Quantum Dot LEDs. *Adv. Mater. Technol.* **2019,** *4* (7), 1800727.

37. Keum, H.; Jiang, Y.; Park, J. K.; Flanagan, J. C.; Shim, M.; Kim, S., Photoresist Contact Patterning of Quantum Dot Films. *ACS Nano* **2018,** *12* (10), 10024-10031.

38. Joo, J.; Na, H. B.; Yu, T.; Yu, J. H.; Kim, Y. W.; Wu, F.; Zhang, J. Z.; Hyeon, T., Generalized and Facile Synthesis of Semiconducting Metal Sulfide Nanocrystals. *J. Am. Chem. Soc.* **2003,** *125* (36), 11100-11105.

39. Korala, L.; Brock, S. L., Aggregation Kinetics of Metal Chalcogenide Nanocrystals: Generation of Transparent CdSe (ZnS) Core (Shell) Gels. *J. Phys. Chem. C* **2012,** *116*, 17110-17117.

40. Yu, W. W.; Qu, L.; Guo, W.; Peng, X., Experimental Determination of the Extinction Coefficient of CdTe, CdSe, and CdS Nanocrystals. *Chem. Mater.* **2003,** *15* (14), 2854-2860.

41. Aresti, A.; Congiu, A.; Manca, P.; Spiga, A., Thermal conductivity of CdS$_x$Se$_{1-x}$ solid solutions. *J. Appl. Phys.* **1973,** *44* (8), 3401-3403.

Table of Contents artwork